Research papers

# Distribution of sea-air $CO_2$ fluxes in the Patagonian Sea: Seasonal, biological and thermal effects

Lucía C. Kahl[a,b,c,*], Alejandro A. Bianchi[a,c], Ana Paula Osiroff[c], Diana Ruiz Pino[d], Alberto R. Piola[a,b,c]

[a] Departamento de Ciencias de la Atmósfera y los Océanos, Facultad de Ciencias Exactas y Naturales, Universidad de Buenos Aires, Buenos Aires, Argentina
[b] Consejo Nacional de Investigaciones Científicas y Técnicas, Buenos Aires, Argentina
[c] Departamento Oceanografía, Servicio de Hidrografía Naval, Buenos Aires, Argentina
[d] Expérimentation et Approches Numériques, Laboratoire d'Océanographie et du Climat, Université Pierre et Marie Curie, Paris, France

## ARTICLE INFO

## ABSTRACT

Sea-air $CO_2$ fluxes ($FCO_2$) in the Patagonian Sea (PS) were studied using observations collected in 2000–2006. Based on the PS frontal structures and the thermal and biological contributions to $FCO_2$ we present a regional subdivision between distinct regimes that provide new insights on the processes that control these fluxes. The coastal regime (CR) is a net source of atmospheric $CO_2$ ($4.9 \times 10^{-3}$ mol m$^{-2}$ d$^{-1}$) while the open shelf regime (SHR) is a net $CO_2$ sink ($-6.0 \times 10^{-3}$ mol m$^{-2}$ d$^{-1}$). The interface between these two regions closely follows the location of along-shore fronts. In addition, based on the nature of the processes that drive the $FCO_2$, the PS is subdivided between northern (NR) and southern (SR) regions. Both, NR and SR are $CO_2$ sinks, but the $CO_2$ uptake is significantly higher in NR ($-6.4 \times 10^{-3}$ mol m$^{-2}$ d$^{-1}$) than in SR ($-0.5 \times 10^{-3}$ mol m$^{-2}$ d$^{-1}$). The data reveal a strong seasonality in $FCO_2$. The mean $CO_2$ capture throughout the PS in austral spring is $-5.8 \times 10^{-3}$ mol m$^{-2}$ d$^{-1}$, reaching values lower than $-50 \times 10^{-3}$ mol m$^{-2}$ d$^{-1}$ in NR, while in winter $FCO_2$ is close to equilibrium in SR. The analysis of the biological and thermal effects (BE and TE, respectively) on seasonal $pCO_2$ variability indicates that regions of $CO_2$ emission are dominated by the TE while regions of $CO_2$ uptake are dominated by the BE. Our results indicate that the biological pump is the dominant process determining the sea-air $CO_2$ flux in the PS.

## 1. Introduction

Carbon dioxide ($CO_2$) is one of the most important greenhouse gases and plays a fundamental role in global warming and ocean acidification. Though marginal seas represent only 7% of the global ocean surface area (Cai, 2011; Walsh, 1988) they account for about 15% of the global ocean $CO_2$ uptake (2.6 PgC yr$^{-1}$, Le Quéré et al., 2016). The role of marginal seas in $CO_2$ dynamics depends on the balance between the capture and regeneration of $CO_2$ in surface waters, the exchanges with the open ocean, and the diversity and abundance of the ecosystems (Borges et al., 2005; Ito et al., 2005). Several studies suggest that air-sea $CO_2$ fluxes in continental shelves capture and export atmospheric $CO_2$ to the open sea (Chen et al., 2004; DeGrandpre et al., 2002; Frankignoulle and Borges, 2001; Tsunogai et al., 1999; Wang et al., 2000). However, their precise contribution to the global ocean budget is still uncertain; with available estimates ranging between 0.19 and 0.45 PgC yr$^{-1}$ (Borges, 2011; Cai et al., 2006; Chen and Borges, 2009; Laruelle et al., 2014; Thomas et al., 2004).

This study is focused on sea-air $CO_2$ fluxes in the western South Atlantic continental shelf from 38 to 55ºS, hereafter referred to as the Patagonia Sea (PS). The PS stands out as one of the most extended and productive shelf regions worldwide (Dogliotti et al., 2014; Lutz et al., 2010). The mean circulation in the PS is dominated by a relatively weak mean flow towards the NNE (referred as Patagonian Current, Brandhorst and Castello (1971)), with a mean transport between 1 and 2 Sv (Palma et al., 2008; Piola and Rivas, 1997; Ruiz Etcheverry et al., 2016). Along the continental shelf break, the Malvinas Current (MC) flows northward, carrying relatively cold, salty (compared with shelf waters) and nutrient rich subantarctic waters. The MC is derived from the northern branch of the Antarctic Circumpolar Current that penetrates northward to about 38ºS along the western margin of the Argentine Basin.

From late spring and early fall the stratification of water column over the PS is induced by surface warming, except for those zones where strong winds and tidal currents (Palma et al., 2008) overcome the effect of the surface heating (Rivas, 2010). Regions with relatively

intense vertical circulation that favor the flow of nutrients through the pycnocline to the illuminated layer, are highly productive (Romero et al., 2006). From early spring to late fall tidal mixing near shore leads to the formation of localized tidal fronts (TF), separating well-mixed coastal waters from stratified waters (Carreto et al., 1995; Glorioso, 1987; Romero et al., 2006). A thermal front referred to as Midshelf Front (MSF) is also observed throughout the year extending from 38 to 42ºS between the 30 and 80 m isobaths (Lucas et al., 2005; Romero et al., 2006). The MSF is associated with a local maximum of Chl-*a* concentration of up to 3 mg m$^{-3}$ during spring (Romero et al., 2006). In addition, an extended termohaline front, referred to as shelf break front (SBF), marks the transition between Malvinas and shelf waters (Acha et al., 2004; Carreto et al., 1986, 1995; Franco et al., 2008; Rivas and Pisoni, 2010). The SBF presents a high Chl-*a* concentration from spring to autumn probably associated with the nutrient-rich waters from the MC (Rivas et al., 2006; Romero et al., 2006).

The sea-air $CO_2$ exchange is controlled by the so-called biological and physical (or solubility) pumps (Volk and Hoffert, 1985). Thermodynamic and kinematic processes govern the physical pump, while the biological pump removes $CO_2$ from the surface waters by phytoplankton photosynthesis. Other processes may transfer $CO_2$ from the surface waters to the deeper ocean and bottom sediments. In the PS the shelf productivity spreads to higher trophic levels reaching top predators, including marine mammals and seabirds (Acha et al., 2004) and benthic communities (e.g. Bogazzi et al., 2005). The intense phytoplankton activity decreases the concentration of inorganic carbon in the upper layer, leading to a strong capture of atmospheric $CO_2$. As a response to these distinct processes the spatial distribution of $CO_2$ fluxes is heterogeneous. Both, sea surface Chl-*a* and sea-air difference in $CO_2$ partial pressure ($\Delta p CO_2$) undergo sharp changes across the tidal fronts (Bianchi et al., 2009). These observations suggest that vertical fluxes associated with ocean fronts promote the growth of phytoplankton in the offshore side of tidal fronts and modulate the $CO_2$ flux through the sea surface. Thus, a link between the dynamics of $p CO_2$, vertical stratification and phytoplankton production is suggested. Therefore, in this study we carry out a regional subdivision between distinct regimes: the coastal and shelf waters (CR and SHR, respectively) and discuss the different $CO_2$ flux regimes that characterize each region.

Horizontal distributions of sea surface temperature (SST) in the PS indicate that there is a relatively sharp temperature transition and amplitude of the SST annual cycle around 47ºS. Several studies show that the amplitude of the seasonal cycle of SST decreases from ~6 ºC at 40ºS to ~2 ºC at 52ºS (Podestá et al., 1991; Rivas, 2010). Summer SST in the north is about 5 ºC higher than in the south (Kahl, 2013), probably due to the combined effect of incoming solar radiation and air-sea heat fluxes (Podestá et al., 1991; Rivas, 2010). Therefore, the stratification of the water column and the light penetration necessary to promote biological activity occur earlier and end later in the north than in the south. According to Romero et al. (2006), in the northern PS, Chl-*a* blooms initiate in early austral spring (September and October), while in the south blooms begin in late spring to early summer (November through January). Away from the shelf break, in the north, the most intense blooms in terms of satellite derived surface Chl-*a* occur along the TF and the MSF, while in the south the high Chl-*a* concentrations are located in Grande Bay (from 52 to 49ºS). The difference between amplitude of the upper layer temperature and the onset of the phytoplankton bloom induces changes in sea-air $\Delta p CO_2$. Thus, in this study we considered a subdivision in northern (NR) and southern regions (SR) at 47ºS.

The main objective of this work is to estimate the thermal and biological contributions to the $p CO_2$ and the resulting $CO_2$ flux through the sea surface, considering a regional subdivision that provides new insights on the processes that control the $CO_2$ fluxes in the PS.

**Table 1**

Details of ARGAU transects and GEF cruises made aboard the Icebreaker Almirante Irízar and the R/V Puerto Deseado respectively.

| Cruise and Transect | Dates |
| --- | --- |
| ARGAU-0 T0 | 24 – 25 March 2000 |
| ARGAU-0 T1 | 27 – 30 March 2000 |
| ARGAU-0 T3 | 11 – 12 May 2000 |
| ARGAU-1 T3 | 24 – 27 January 2001 |
| ARGAU-1 T4 | 19 – 21 February 2001 |
| ARGAU-1 T8 | 5 – 8 April 2001 |
| ARGAU-1i T1 | 8 – 10 August 2001 |
| ARGAU-1i T2 | 12 – 15 August 2001 |
| ARGAU-2 T1 | 31 January to 2 February 2002 |
| ARGAU-2 T6 | 23 – 27 March 2002 |
| ARGAU-2 T7 | 10 – 13 April 2002 |
| ARGAU-2 T10 | 3 – 5 May 2002 |
| ARGAU-3 T1 | 7 – 10 February 2003 |
| ARGAU-3 T10 | 15 – 18 May 2003 |
| ARGAU-4 T7 | 27 February to 1 March 2004 |
| ARGAU-4 T8 | 13 – 16 March 2004 |
| ARGAU-4 T11 | 14 – 18 April 2004 |
| ARGAU-5 T1 | 25 – 28 December 2004 |
| ARGAU-5 T9 | 9 – 12 April 2005 |
| GEF 1 | 9 – 28 October 2005 |
| GEF 2 | 10 March to 01 April 2006 |
| GEF 3 | 7 – 25 September 2006 |

## 2. Data and methods

### 2.1. Data acquisition

In this article we use air and seawater $p CO_2$, Chl-*a*, fluorescence, sea surface salinity (SSS), SST, air humidity, atmospheric pressure and, in some cases, total $CO_2$ ($TCO_2$) and alkalinity (TA) obtained over the PS during 10 cruises carried out from 2000 to 2006 (Table 1 and Fig. 1). The cruises were carried out within the framework of the program of cooperation France-Argentina (ARGAU, 2000–2005) and a national project sponsored by the "Global Environmental Facility" (GEF-Patagonia, 2005–2006), within the framework of a UNESCO program (PNUD-AR-02/018; e.g. Charo and Piola (2014)).

In all the cruises, the SST and SSS were recorded continuously, using Sea-Bird Electronics 21 and 37 SI sensors. The measurements of $p CO_2$ of seawater and air were made with an IR analyzer, except for a small number of samples corresponding to cruise GEF1 as explained later. The $p CO_2$ system is a semi-continuous system of equilibrated flux with a Siemens Ultramat 5F IR analyzer (Metzl et al., 1995). The system is fed by a constant seawater flux that is pumped from an outlet located in the ship's hull at a depth of 3.5 m (GEF cruises) and 9 m (ARGAU cruises). Because the depth of the mixed layer in the PS is larger than 20 m, except in CR and winter where water column is homogeneous, the difference in the intake depths is not expected to introduce a significant bias in our estimates of seawater $p CO_2$. Each $p CO_2$ observation is the average of 60 measurements taken over a period of 10 min. The standard deviation of seawater $p CO_2$ observations was about 1 μatm, except across frontal zones, where higher spatial variability led to increased standard deviations. The system was calibrated every six hours with 3 gas standards of 270.0, 361.0 and 489.9 ppm to monitor and eliminate drifts in the IR analyzer. Seawater $p CO_2$ was corrected for warming effects using temperature data obtained from high-accuracy sensors placed in the equilibrator and in the seawater intake. The air $p CO_2$ samples were collected at six hour intervals from the bow of the ship to avoid contamination. In addition, air $p CO_2$ was corrected for atmospheric pressure and air humidity effects. During the first 8 days of the GEF1 cruise the seawater $p CO_2$ could not be measured with the IR analyzer due to a system malfunction. Therefore, during this time period $p CO_2$ was estimated from $TCO_2$
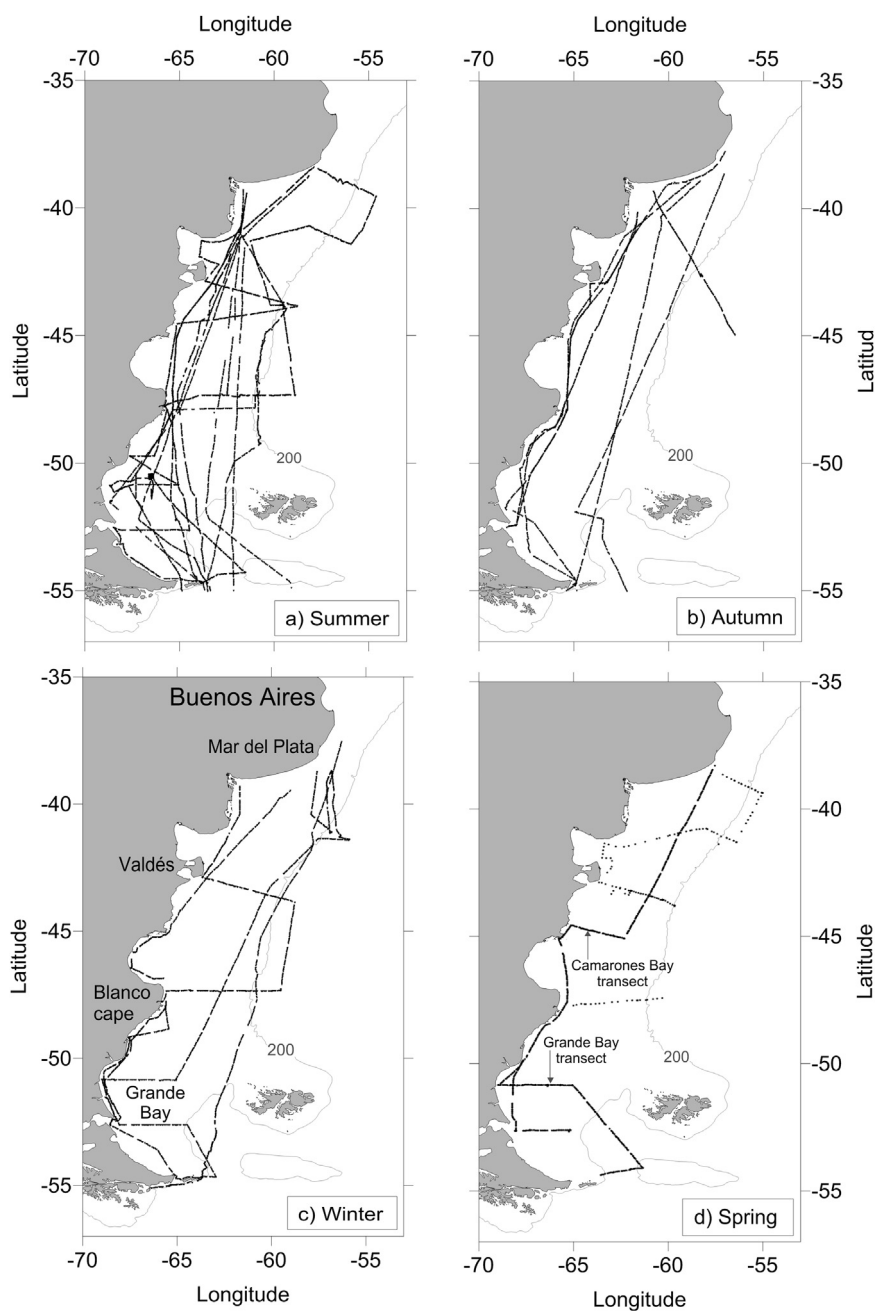
**Fig. 1.** Tracks of the ARGAU (2000 – 2005) and GEF cruises (2005 – 2006). a) Summer (January to March), b) autumn (April and May), c) winter (August and September) and d) spring (October).

and TA, using the CO2SYS program (Pierrot et al., 2006). TCO$_2$ and TA were determined with a potentiometric method following Gran (1952). After 2009 a data quality control led to slight change in AT and $p$CO$_2$ calculated using CO2SYS. Thus annual mean sea-air difference of $p$CO$_2$ ($\Delta p$CO$_2$) presented in this paper differ in 1.7 ± 4 µatm from the annual mean $\Delta p$CO$_2$ reported by Bianchi et al. (2009). This difference is not significant since it is smaller than the standard error of the mean value (± 4 µatm).

In the ARGAU cruises, the Chl-*a* concentration was determined from 1.5 to 2 l of seawater samples, which were filtered using Whatman GF/F, frozen (−20 ºC) and stored in a dark environment. After thawing, the pigments were extracted by placing the filters in 8 ml of 90% acetone. The material extracted was read spectrophotometrically with a Beckman DU 650 spectrophotometer. Pigment concentration calculations were conducted according to Strickland and Parsons (1972). In the three GEF

cruises, surface Chl-*a* was determined from seawater samples filtered with glass fiber-filters similar to Whatman GF/F, and kept in liquid nitrogen (−196 ºC) on board. In these cruises Chl-*a* samples were also taken at all CTD stations and every 2 h underway. The Chl-*a* was analyzed by the fluorometric method of Holm-Hansen et al. (1965) modified by Lutz et al. (2010). The pigments were extracted in 100% methanol and read with a Perkin Elmer LS3 spectrofluorometer.

A total of 3163 hydrographic stations occupied over the continental shelf during austral summer (December to March) between 1926 and 2010 obtained from the US NODC World Ocean Database 2013 (WOD13: https://www.nodc.noaa.gov/OC5/WOD/pr_wod.html (Boyer et al., 2013)) and Base Regional de Datos Oceanográficos (BaRDO: http://www.inidep.edu.ar/oceanografia/) were used to determine the Simpson Parameter (Simpson, 1981).

## 2.2. Biological and thermal effects

To determine the relative importance of the biological and thermal effects (BE and TE, respectively) on the changes of $pCO_2$ in sea water, we follow the approach proposed by Takahashi et al. (2002). To remove the temperature effect on seawater $pCO_2$, the data were normalized to the annual mean in-situ SST in the region of study, according to Eq. (1). When the temperature effect is removed, the remaining variations in $pCO_2$ are due to BE, which includes the effects of the net biological utilization of $CO_2$ and other processes, including the vertical and lateral transport and sea-air exchange of $CO_2$ (see Discussion).

$$(pCO_2 \, atSST_{mean}) = (pCO_{2obs}) \cdot \exp[0.0423 \cdot (SST_{mean} - SST_{obs})] \quad (1)$$

The subscripts "mean" and "obs" indicate the annual averaged and observed values, respectively. The temperature effect on $pCO_2$ ($\partial \ln pCO_2/\partial SST = 0.0423 \, °C^{-1}$) was determined based on the analysis of surface waters from the North Atlantic (Takahashi et al., 1993), which is nearly independent of the temperature and chemical composition of seawater (Rubin, 2000).

Effects of the temperature changes in the seawater $pCO_2$ have been computed by perturbing the mean annual $pCO_2$ with the difference between the mean and observed temperature. The $pCO_2$ at an observed temperature ($SST_{obs}$) was calculated based on Eq. (2).

$$(pCO_2 \, atSST_{obs}) = (pCO_{2MeanAnnual}) \cdot \exp[0.0423 \cdot (SST_{obs} - SST_{mean})] \quad (2)$$

Annual mean estimates of SST and seawater $pCO_2$ were determined from in-situ data. Taking into account the regional subdivision in NR and SR, based on 10600 SST and $pCO_2$ observations, the mean SST and $pCO_2$ are 11.9 °C and 340 µatm in NR and 8.1 °C and 365 µatm, in SR, respectively.

## 2.3. Simpson parameter

The Simpson parameter ($\Phi$) is a measure of the energy required to mix the water column. $\Phi$ is defined as:

$$\Phi = \frac{g}{h} \int_h^0 (\rho - \rho_0) \cdot z \cdot dz, \quad (3)$$

where $g$ is the gravitational acceleration, $h$ is the depth of the water column, $\rho$ is the density of seawater, and $\rho_0$ is the mean density of the water column. Thus, $\Phi$ provides a simple quantitative measure of the vertical stratification that allows a subdivision between stratified and well-mixed shelf waters (Fig. 2), associated with the SHR and CR respectively. A critical value of $\Phi c = 50 \, J \, m^{-3}$ was adopted to separate stratified ($\Phi > 50 \, J \, m^{-3}$) from well-mixed waters ($\Phi < 50 \, J \, m^{-3}$). $\Phi c = 50 \, J \, m^{-3}$ closely matches the mean location of the TF and MSF. Though previous studies have estimated the Simpson parameter to determine the degree of stratification of the PS (e.g. Bianchi et al., 2005; Sabatini et al., 2000, 2004, 2012, among others), here $\Phi c$ was estimated using a significantly updated data set.

## 2.4. Calculation of the sea-air $CO_2$ flux

The net sea-air $CO_2$ flux ($FCO_2$) was estimated using the relation:

$$FCO_2 = k_w \cdot k_s \cdot \Delta pCO_2, \quad (4)$$

where $k_w$ is the gas transfer velocity, $k_s$ is the coefficient of solubility of $CO_2$ in seawater, and $\Delta pCO_2$ is the sea-air difference of $pCO_2$ ($pCO_{2sea} - pCO_{2atm}$). $k_s$ was calculated according to the expression proposed by Copin-Montégut (1996) and $k_w$ following Wanninkhof (2014). To calculate the surface fluxes we used Cross-Calibrated Multi-Platform (CCMP) winds available at 6-h intervals and 0.25° resolution (Atlas et al., 2011) obtained from the Physical Oceanography Distributed Active Archive Center of the Jet Propulsion Laboratory (PO.DAAC, JPL, NASA, http://podaac.jpl.nasa.gov/DATA_CATALOG/ccmpinfo.html).
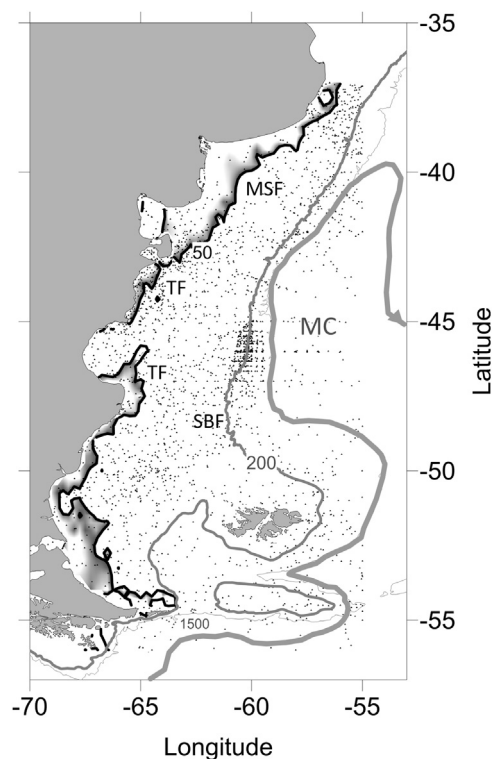


**Fig. 2.** Location of SBF, TF, MSF and Malvinas Current (MC). The 200 m isobaths is used to indicate the location of the SBF. The location of the TF and the MSF are represented by the critical Simpson parameter $\Phi c = 50 \, J \, m^{-3}$ and MC location is extracted from Piola et al. (2013). Dots show the location of historical hydrographic data used to calculate de Simpson parameter.

## 3. Results

### 3.1. Biological and thermal effects on $pCO_2$

Fig. 3 illustrates the seasonal variation of in-situ SST (crosses and solid line) and sea water $pCO_2$ (dots and dashed line), for NR and SR. The seasonal variation of in-situ SST in SR is about 3 °C smaller than the seasonal variation in NR and the SST maxima occur in January at NR and in February at SR. Though in both, NR and SR the sea surface $pCO_2$ maxima occur in May, the minima are observed in October at NR and in December at SR. Thus, seasonal $pCO_2$ changes are not in phase with SST, indicating that the changes in $pCO_2$ are not dominated by temperature changes.

Monthly means of BE and TE on $pCO_2$ are presented in Fig. 4. In our $pCO_2$ data set no observations were collected in June, July and November (see Table 1). In both NR and SR, the BE on $pCO_2$ is low in austral summer (i.e. January) and high in winter (i.e. August) while the annual cycle of the TE presents an opposite pattern (high in summer and low in winter).

The relative importance of BE and TE is represented by the difference between their seasonal amplitudes ($\Delta A = A_{TE} - A_{BE}$). The seasonal amplitude of TE is 137 µatm at NR and 97 µatm at SR while the amplitudes of the BE are 170 µatm at NR and 154 µatm at SR. Both regions present negative $\Delta A$ (−33 and −57 µatm, in NR and SR, respectively), indicating that the BE dominates the seasonal $pCO_2$ variability. In addition, on average, in NR the BE is less significant than in SR. This could be due to the larger SST amplitude (~9 °C vs. 6 °C) in NR compared to SR (Fig. 3).

The surface distribution of the annual mean difference between TE and BE ($\Delta A$) is presented in Fig. 5. In the mid and outer PS (SHR), the differences are mostly negative (BE > TE) showing the dominance of BE (mean $\Delta A = -27.7 \pm 2$ µatm). However, in the inner shelf (CR),
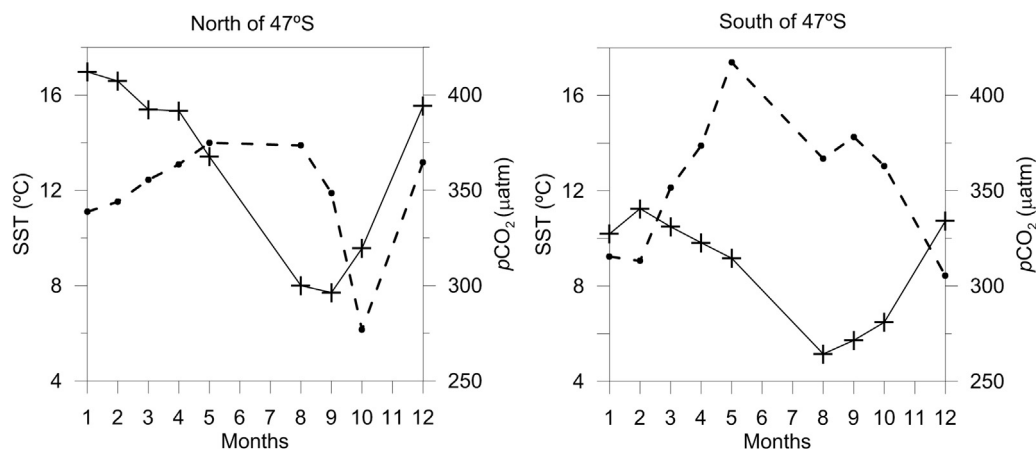
**Fig. 3.** Annual cycle of seawater $pCO_2$ (dashed line) and SST during 2000–2006 (solid line) in the NR (left) and SR (right).

positive values are observed, with a mean $\Delta A$ of 30 ± 5 µatm. Particularly high $\Delta A$ is observed in the CR, from 38 to 41°S, west of the MSF ( > 70 µatm).

### 3.2. Regional variability of pCO₂ and FCO₂

Seasonal and annual mean $\Delta pCO_2$ and $FCO_2$ of the sub-regions (CR, SHR, NR and SR) are presented in Tables 2, 3. Positive and negative values of $\Delta pCO_2$ and $FCO_2$ correspond to sources and sinks of atmospheric $CO_2$, respectively. The standard errors of $\Delta pCO_2$ and $FCO_2$ range between 1 and 7 µatm and $< 2 \times 10^{-3}$ mol m$^{-2}$ d$^{-1}$, respectively (Tables 2 and 3). Seasonal surface $FCO_2$ distributions are shown in Fig. 6. The main features of these fields are described below.

#### 3.2.1. Coastal region

In the CR the annual mean $FCO_2$ is $4.9 \times 10^{-3}$ mol m$^{-2}$ d$^{-1}$ which leads to an annual $CO_2$ emission of 4 TgC yr$^{-1}$. During summer and autumn the $CO_2$ emission at CR is high (mean $\Delta pCO_2 \sim$ 38 µatm) and presents a relatively homogeneous distribution (Table 2 and Fig. 6). Moreover, the transition from $CO_2$ emission to uptake matches the critical Simpson parameter (Figs. 2 and 6), indicating the importance of vertical mixing on the sign of $FCO_2$. The surface distribution of in-situ Chl-$a$ in CR indicates a rich phytoplankton biomass associated with strong spring blooms (Bianchi et al., 2009; Lutz et al., 2010). Likewise, the mean $FCO_2$ in spring is negative ($-1.0 \times 10^{-3}$ mol m$^{-2}$ d$^{-1}$) due to the strong bloom widely extended over the

CR. Nevertheless, from spring to autumn the highest emission values are observed adjacent to Valdés Peninsula. In winter the net $CO_2$ exchanged with the atmosphere in the CR is low, with mean $\Delta pCO_2$ of 5 µatm. The maximum $\Delta pCO_2$, which reaches 122 and 130 µatm, are observed close to the north coast of Valdés Peninsula ($\sim$42°S–64.5°W) in summer and in Grande Bay ($\sim$51–53°S) in autumn, respectively.

#### 3.2.2. Shelf region

The observed annual mean $FCO_2$ in the SHR indicates an intense uptake ($-6.0 \times 10^{-3}$ mol m$^{-2}$ d$^{-1}$) which is equivalent to a mean annual carbon flux of $-20$ TgC yr$^{-1}$ into the ocean. The mean $FCO_2$ over the SHR indicates $CO_2$ capture throughout the year. From spring to autumn, the uptake is intense, reaching $-7.4 \times 10^{-3}$ mol m$^{-2}$ d$^{-1}$ in autumn, and is lowest in winter ($-2.6 \times 10^{-3}$ mol m$^{-2}$ d$^{-1}$). It should be kept in mind that the TF vanishes during winter due to net the heat flux to the atmosphere and subsequent convection which leads to intense vertical mixing that destroys the stratification even in the mid-shelf region (Rivas and Piola, 2002). Hence, during winter, the contrast in stratification between CR and SHR is negligible and the $FCO_2$ difference is significantly reduced (Table 2).

#### 3.2.3. Northern region

The seasonal surface distributions of $FCO_2$ show that the NR is a sink of atmospheric $CO_2$ throughout the year (Fig. 6, Table 3). The $FCO_2$ annual mean in this region ($-6.4 \times 10^{-3}$ mol m$^{-2}$ d$^{-1}$) is equivalent to net flux of $-15$ TgC yr$^{-1}$ into the ocean. The maximum
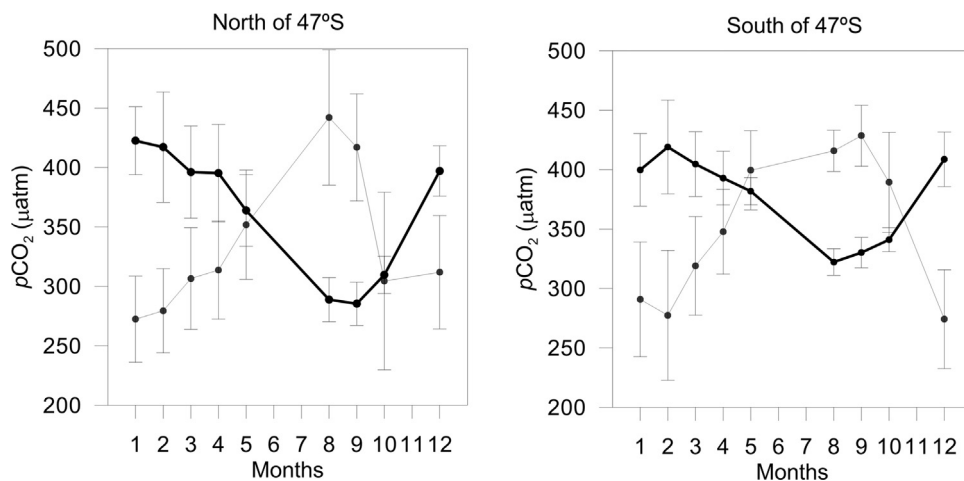


**Fig. 4.** Annual cycle of seawater $pCO_2$ due to BE (grey) and TE (black) in the NR (left) and SR (right). The vertical bars indicate standard deviations around each monthly mean.
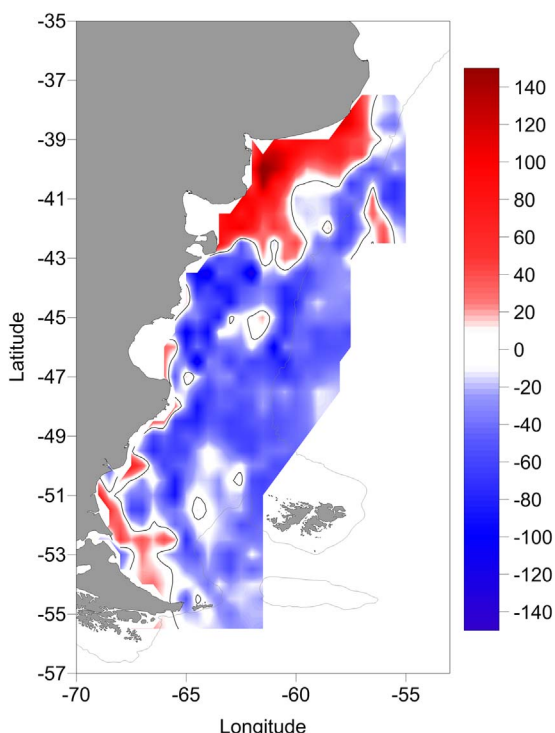
**Fig. 5.** Difference between the effects of seasonal temperature changes and biology (TE - BE, in µatm) on $p$CO$_2$. Negative values indicate that BE dominates the $p$CO$_2$ variability. Contour of TE − EB = 0 is shown.

**Table 2**

Seasonal and annual mean values of $\Delta p$CO$_2$ (µatm), FCO$_2$ ($10^{-3}$ mol m$^{-2}$ d$^{-1}$), and standard errors[a] for CR, SHR and the full domain.

| | CR | | SHR | | Total Region |
|---|---|---|---|---|---|
| | $\Delta p$CO$_2$ | FCO$_2$ | $\Delta p$CO$_2$ | FCO$_2$ | FCO$_2$ |
| Summer | 39 ± 6 | 6.3 ± 1.1 | −44 ± 2 | −6.8 ± 0.6 | −4.3 ± 0.6 |
| Autumn | 38 ± 4 | 11.0 ± 1.7 | −38 ± 3 | −7.4 ± 0.7 | −3.2 ± 0.9 |
| Winter | 5 ± 3 | 3.4 ± 1.3 | −9 ± 2 | −2.6 ± 0.8 | −1.3 ± 0.7 |
| Spring | −16 ± 7 | −1.0 ± 0.6 | −74 ± 4 | −7.1 ± 0.4 | −5.8 ± 1.0 |
| Annual | 17 ± 7 | 4.9 ± 1.7 | −41 ± 4 | −6.0 ± 0.8 | −3.7 ± 1.0 |

[a] Standard error:$\varepsilon = Zx\sigma/(N)^{1/2}$, where Z = 3 for a significance level of 99.73, σ is the sample standard deviation and N is the number of data used.

**Table 3**

Seasonal and annual mean values of $\Delta p$CO$_2$ (µatm), FCO$_2$ ($10^{-3}$ mol m$^{-2}$ d$^{-1}$) and standard errors for NR, SR, and full domain.

| | NR | | SR | | Total Region |
|---|---|---|---|---|---|
| | $\Delta p$CO$_2$ | FCO$_2$ | $\Delta p$CO$_2$ | FCO$_2$ | FCO$_2$ |
| Summer | −24 ± 4 | −3.2 ± 0.9 | −34 ± 3 | −5.3 ± 0.2 | −4.3 ±0.6 |
| Autumn | −32 ± 4 | −8.4 ± 1.1 | −1 ± 3 | 3.1 ± 1.4 | −3.2 ± 0.9 |
| Winter | −14 ± 5 | −3.8 ± 1.1 | −0.2 ± 1 | 1.6 ± 0.7 | −1.3 ± 0.7 |
| Spring | −98 ± 6 | −10.0 ± 1.8 | −22 ± 3 | −1.3 ± 0.3 | −5.8 ± 1.0 |
| Annual | −42 ± 6 | −6.4 ± 2 | −14 ± 3 | −0.5 ± 0.4 | −3.7 ± 1.0 |

seasonal CO$_2$ uptake is observed in spring (Fig. 6d, Table 3), with seasonal mean values of $\Delta p$CO$_2$ and FCO$_2$ as high as −98 µatm and −10.0 × $10^{-2}$ mol m$^{-2}$ d$^{-1}$, respectively. Concurrent Chl-$a$ and $\Delta p$CO$_2$ observations collected in October 2005, which are representative of the spring bloom, suggest that the biological pump is important. For example, data collected in spring along a zonal section around 45°S (Camarones Bay transect, see Fig. 1 for location), show that Chl-$a$ and $\Delta p$CO$_2$ are significantly anti-correlated (R$^2$ = 0.78), with maximum Chl-$a$ (8 mg m$^{-3}$) co-located with a minimum of $\Delta p$CO$_2$ (−231 µatm)

(Fig. 7a). In summer, the CO$_2$ uptake by phytoplankton decreases, associated with the nutrient uptake in the surface layer during the preceding spring (Carreto et al., 1995).

*3.2.4. Southern region*

Seasonal distributions of surface FCO$_2$ in the SR are presented in Fig. 6. In autumn and winter, the sea-air FCO$_2$ indicates emission of CO$_2$ to the atmosphere. Nevertheless, during autumn, the FCO$_2$ surface distribution shows a clear difference between two regions: the coastal and a mid-shelf zones present positive and negative values, respectively, while in winter the distribution is more homogeneous, with lower values than observed in the other seasons (−5 to 5 × $10^{-3}$ mol m$^{-2}$ d$^{-1}$). Generally, during the cold period (winter and autumn) the surface Chl-$a$ is low (< 1 mg m$^{-3}$), except near ~50°S–67°W during autumn, where Chl-$a$ concentrations reach values of 11 mg m$^{-3}$associated with a $\Delta p$CO$_2$ of −53 µatm. The stronger CO$_2$ sink observed in summer (Fig. 6a, FCO$_2$ = −5.3 × $10^{-3}$ mol m$^{-2}$ d$^{-1}$), is associated with slightly higher Chl-$a$ than observed in the NR during that season. During spring, the $\Delta p$CO$_2$ in the SR is about 20% of the $\Delta p$CO$_2$ observed in NR. Data collected in October 2005 along a cross-shelf section of Chl-$a$ and $\Delta p$CO$_2$ off Grande Bay reveal a maximum CO$_2$ uptake ($\Delta p$CO$_2$ = − 190 µatm) associated with a strong bloom (Chl-$a$ = 28.6 mg m$^{-3}$) (Fig. 7b). The SR annual mean sea-air CO$_2$ flux is −0.5 × $10^{-3}$ mol m$^2$ d$^{-1}$ which leads to an annual mean uptake of −1 TgC yr$^{-1}$.

## 4. Discussion

Our results indicate that the $p$CO$_2$ variability over most of the PS is dominated by the BE, which includes the net biological CO$_2$ utilization and other processes such as advection and vertical and lateral turbulent mixing. These processes have been analyzed using numerical models. In the surface of the shelf break region, Lagrangian simulations of passive particles showed intense vertical velocities. Passive particles released in the upper layer in these high-resolution models reach the bottom at ~ 200 m depth (Franco et al., 2017), suggesting relatively intense downwelling. Such vertical coupling is supported by the observation of high concentration of diatoms in gut contents of benthic filter-feeding scallops located on the bottom along the outer shelf (Schejter et al., 2002). These relatively intense downwelling cells may effectively transfer carbon below the mixed layer. On the other hand, numerical (Matano and Palma, 2008) and analytical models (Miller et al., 2011), and observations (Valla and Piola, 2015) indicate that relatively intense upwelling also occurs in the vicinity of the shelf break. In the models, shelf break upwelling is controlled by the along-shelf pressure gradient associated with the downstream divergence of a slope current. The intensity of the upwelling is modulated by the strength of the slope current (Matano and Palma, 2008). This modulation is also suggested by observations of intense upper ocean cooling along hundreds of kilometers of the outer shelf and slope during sharp accelerations of the along-slope flow (Valla and Piola, 2015). Though area-averaged shelf break upwelling is confirmed by realistic, high-resolution simulations (Combes and Matano, 2014), the models also show a complex pattern of vertical circulation, with intense, small-scale upwelling and downwelling cells. Upwelling provides a source of macronutrients and probably the dissolved iron needed to sustain large diatom blooms during spring (Carreto et al., 2016). Though upwelling of carbon-rich subsurface waters would transfer carbon to the upper layer, the associated upward nutrient flux promotes the growth of phytoplankton which enhances the biological carbon uptake. Thus, the intense vertical circulations near the shelf break may favor carbon uptake in the surface layer in upwelling cells and carbon transfer to the lower layer in downwelling cells.

The increase of the surface ocean $p$CO$_2$ in winter in both NR and SR, after removing the temperature effect (Fig. 4), could be partly due to vertical mixing after the intense stratification is destroyed by wind
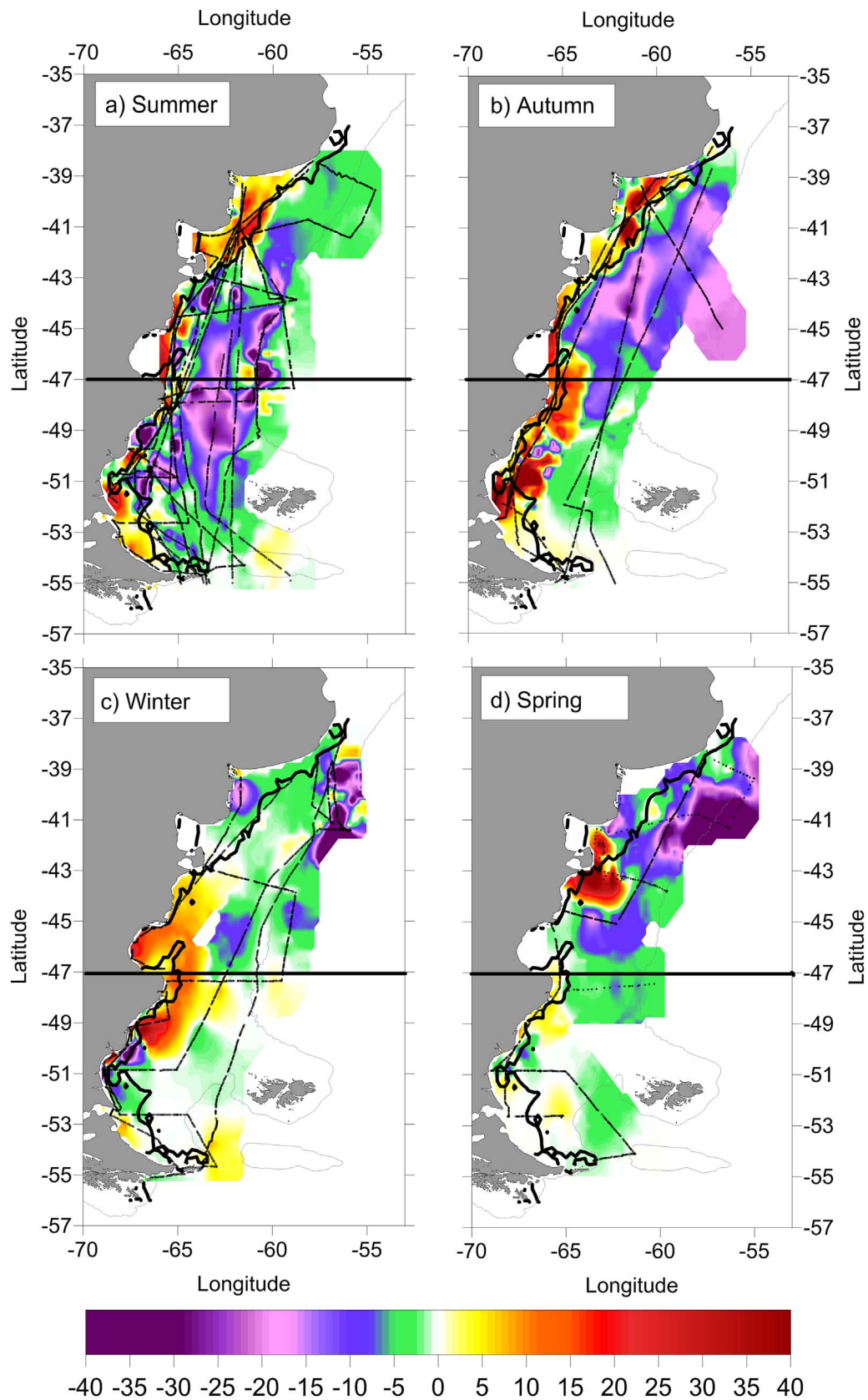
**Fig. 6.** Seasonal surface distributions of FCO$_2$ ($10^{-3}$ mol m$^{-2}$ d$^{-1}$). The thick line indicates the critical Simpson parameter ($\Phi c$ = 50 J m$^{-3}$) separating CR and SHR. Also shown are the 47ºS parallel, which marks the limit between NR and SR, and the 200 m isobath (grey). Black points indicate the tracks of the ARGAU and GEF cruises.
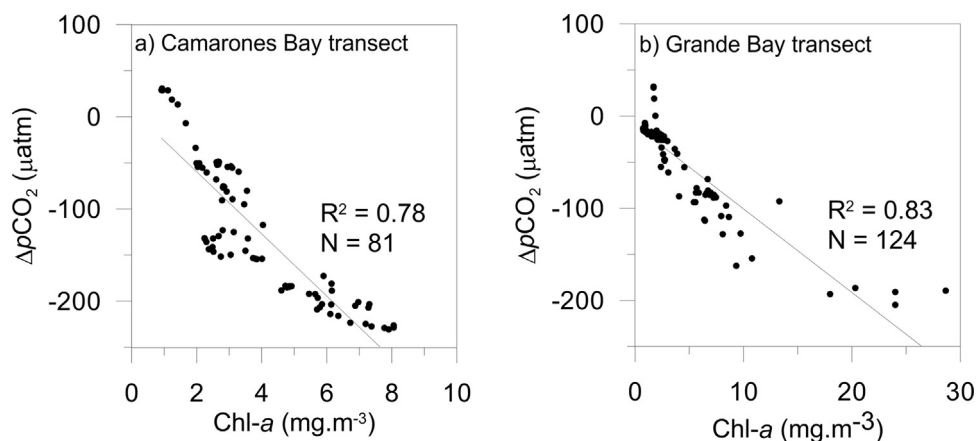
Fig. 7. Surface $\Delta pCO_2$ (µatm) vs Chl-$a$ (mg m$^{-3}$) for Camarones Bay (a) and Grande Bay (b) transects. R is the linear correlation coefficient and N the number of samples.

mixing and convection associated with heat loss to the atmosphere (see Rivas and Piola, 2002). Due to the sparse observations of subsurface carbon concentration we are unable to accurately estimate the impact of vertical mixing. Though the surface $pCO_2$ starts increasing in January at NR (Fig. 3), hydrographic observations collected north of 47°S present strong vertical stratification in the mid and outer shelf through late March (Bianchi et al., 2009; Valla and Piola, 2015), suggesting that the increase of $pCO_2$ is not caused by vertical mixing in that region.

The near neutral surface $CO_2$ balance in winter throughout the PS (Tables 2 and 3) suggest that the carbon uptake during the other seasons is either transferred to the sediments over the shelf (e.g. Gómez et al., 2011) or exported to the open ocean. In-situ and altimeter based observations (Rivas, 1997; Ruiz Etcheverry et al., 2016) and numerical models (Palma et al., 2008) indicate that the mean flow over the mid and outer shelf is ~0.1 m s$^{-1}$ towards the NNE. Moreover, water mass analyses (Piola et al., 2008), altimeter derived currents (Strub et al., 2015) and realistic high-resolution models (Matano et al., 2014) indicate that most of the shelf waters of southern origin are exported offshore north of 38°S. Even at moderate speeds of 0.1 m s$^{-1}$, it would take less than 6 months for shelf waters to be advected 1500 km towards the NNE and exported to the deep ocean. Thus, it is likely that at least a fraction of the carbon absorbed by the PS in spring-summer is exported northward and flushed offshore prior to the following winter. Consequently, the sub-thermocline waters exposed to the atmosphere every winter as a result of wind mixing and heat lost to the atmosphere do not present the high carbon concentrations that would be expected based on the high uptake rates observed in the PS during the remaining of the year.

Our results are in agreement with Takahashi et al. (2002), who also reported high biological activity and strong $CO_2$ uptake in the PS based on much sparser data. In addition, satellite images of the world's oceans indicate that the PS is one of the areas of highest Chl-$a$ concentration (Lutz et al., 2010). Numerical biogeochemical experiments indicated that the subsurface waters from the southeast Pacific are the most important nutrient source to the southwest Atlantic, particularly to the southern Patagonian Shelf (Song et al., 2016). These nutrient rich waters could support phytoplankton blooms and the high net $CO_2$ uptake resulting in PS.

Though the biological effect plays a dominant role on the $pCO_2$ in the PS, the TE dominates the seawater $pCO_2$ variations between the coast and the MSF (Fig. 5), where the highest $CO_2$ emission is observed, mainly during summer and autumn (Fig. 6a, b). The probable cause for this high $CO_2$ emission is the low Chl-$a$ (between 39–41°S), which in turn is associated with weak vertical stratification, as indicated by the critical Simpson parameter $\Phi < 50$ J m$^{-3}$ (Fig. 2), and a nitrate deficit during these seasons (Carreto et al., 1995; Romero

et al., 2006; Marrari et al., 2013).

Our results indicate that the biological activity dominates the $CO_2$ flux distribution in SHR. From spring to autumn, maximum $CO_2$ uptake is observed along the shelf break front. High Chl-$a$ is evident in satellite images in frontal areas (Romero et al., 2006), mainly at the shelf-break (up to 19.0 mg m$^{-3}$), associated with the highest integrated net primary production in the northern portion of the shelf-break front (Garcia et al., 2008; Lutz et al., 2010). A distinct $CO_2$ uptake maximum is observed in the SHR, at Grande Bay (~51°S) during the warm period (from October to May), when waters are moderately stratified. These intense southern Patagonia blooms are associated with increased biomass of autotrophic dinoflagellates (Gómez et al., 2011). In the southern Grande Bay, a sharp decline in phytoplankton abundance was evident coinciding with the occurrence of well-mixed, coastal waters (Sabatini et al., 2000, 2012).

The PS is a net sink of atmospheric $CO_2$ like other continental shelves such as North Sea (Thomas et al., 2004; Prowe at al, 2009), Bering Sea (Bates et al., 2011), Chukchi Sea (Bates, 2006; Evans et al., 2015), East China Sea (Guo et al., 2015; Kim et al., 2013; Tsunogai et al., 1999; Wang et al., 2000), among others. Particularly, our net annual mean FCO$_2$ estimate over the PS (–1.35 mol m$^{-2}$ yr$^{-1}$) is similar to that reported in the North Sea (–1.64 mol m$^{-2}$ yr$^{-1}$, (Thomas et al., 2004)). The contrast between the $CO_2$ outgassing from the well-mixed regions along the coastal band and the $CO_2$ uptake characteristic of the stratified mid and outer shelf regions in the PS resembles the contrast between the northern and southern North Sea. In agreement with our results in the PS, the net $CO_2$ uptake in the seasonally stratified northern North Sea is high due to high net community production in the surface water, while in the permanently mixed southern region, dominated by a weak net $CO_2$ source, the $pCO_2$ cycle appears to be controlled by temperature variations (Prowe et al., 2009). Biological processes also dominate the seasonal dynamics of $CO_2$ in the Bering Sea, although the $CO_2$ uptake estimated in 2008 was 157 TgC yr$^{-1}$ (Bates et al., 2011) is an order of magnitude larger than in the PS. This very high $CO_2$ sink is due to the ice retreat from late spring to summer, which leads to high rates of net community production particularly within the "green belt" area of the Bering Sea shelf (Mathis et al., 2010).

Coastal bays along the eastern US, including the South Atlantic Bight (SAB) and Middle Atlantic Bight (MAB), have some similarities with the PS: relatively strong seasonal stratification and a shelf break front with a western boundary current that influences the shelf productivity. The annual mean $CO_2$ flux estimated in this work for the CR (4.9 × 10$^{-3}$ mol m$^{-2}$ d$^{-1}$, Table 2) is similar to the 3.3 × 10$^{-3}$ mol m$^{-2}$ d$^{-1}$ estimated in the inner shelf in the SAB (Jiang et al., 2008) but the $CO_2$ uptake in the SHR (–6.0 × 10$^{-3}$ mol m$^{-2}$ d$^{-1}$, Table 2) is about twice the value estimated in the middle and outer

SAB. The different $CO_2$ uptake between SHR and SAB is possibly due to the difference in both ecosystems that are dominated by autotrophic and heterotrophic organisms, respectively (Schloss et al., 2007; Cai et al., 2003). In addition, in contrast with the SAB, which is bounded by oligotrophic Gulf Stream waters, the PS is bounded by the high-nutrient, low-chlorophyll MC (Garcia et al., 2008; Signorini et al., 2009). On the other hand, DeGrandpre et al. (2002) found that as a result of seasonal cooling and heating and due to an asymmetry in the wind speed distribution, the MAB is a net sink for atmospheric $CO_2$. In contrast with the PS, where the sea-air $CO_2$ fluxes are controlled by the BE, over the MAB and SAB the $CO_2$ fluxes seem to be dominated by temperature change effects (by DeGrandpre et al., 2002; Jiang et al., 2008).

On the basis of our $pCO_2$ observations and estimated $CO_2$ fluxes, the CR in the PS is a net source of $CO_2$ to the atmosphere ($4.9 \times 10^{-3}$ mol m$^{-2}$ d$^{-1}$) while the SHR is a net $CO_2$ uptake region ($-6.0 \times 10^{-3}$ mol m$^{-2}$ d$^{-1}$). In their synthesis of global $pCO_2$ observations in marginal seas, Chen and Borges (2009) concluded that most open shelves in temperate and high-latitude regions are under-saturated with respect to atmospheric $CO_2$ throughout the year, and that near-shore waters are $CO_2$ sources to the atmosphere. Thus, our results are in good qualitative agreement with Chen and Borges (2009).

## 5. Summary and conclusions

Based on $pCO_2$ data collected from 2000 to 2006, we analyzed the spatial and seasonal variability of $FCO_2$ in the southwest South Atlantic shelf. The interannual variability was not studied in the present work because our data are too sparse spatially and temporarily to assess an impact of that scale. Based on the hydrographic conditions and the nature of the $pCO_2$ variability the domain was subdivided in coastal and shelf sub-regions (CR and SHR) and in north and south sub-regions (NR and SR). Our main conclusions are:

- The annual mean difference between the thermal (TE) and biological effects (BE) on seawater $pCO_2$ in the PS is $-43$ µatm, indicating that the biological pump is the dominant process determining the sea-air $CO_2$ flux in the PS.
- The TE is the dominant process in the coastal region (CR) while the BE is the dominant process in shelf region (SHR). The CR is a source of atmospheric $CO_2$ with a mean annual flux of $4.9 \times 10^{-3}$ mol m$^{-2}$ d$^{-1}$, which leads to net $CO_2$ flux of 4 TgC yr$^{-1}$. The highest emissions occur during summer and autumn. On the other hand, the SHR presents a strong sink of atmospheric $CO_2$ $-6.0 \times 10^{-3}$ mol m$^{-2}$ d$^{-1}$, equivalent to $-20$ TgC yr$^{-1}$, with the maximum uptake occurring in spring.
- The Northern Region annual mean $CO_2$ uptake is $-6.4 \times 10^{-3}$ mol m$^{-2}$ d$^{-1}$ ($-15$ TgC yr$^{-1}$) ranging between $-10.0 \times 10^{-3}$ mol m$^{-2}$ d$^{-1}$ during spring and $-3.2 \times 10^{-3}$ mol m$^{-2}$ d$^{-1}$ during summer. The $CO_2$ uptake decreases substantially in the Southern Region (SR), with an annual mean $FCO_2$ of $-0.5 \times 10^{-3}$ mol m$^{-2}$ d$^{-1}$ ($-1$ TgC yr$^{-1}$). The maximum $CO_2$ flux in the SR, $-5.3 \times 10^{-3}$ mol m$^{-2}$ d$^{-1}$, is observed in austral summer, while in winter and autumn the $CO_2$ flux is to the atmosphere. Differences in stratification between NR and SR and a lag in the onset of the spring bloom in SR, due to lower incident solar radiation, are the most likely causes for the weaker ocean-atmosphere $CO_2$ fluxes observed in SR.

The PS presents high biological activity stimulated by intense wind and tidal mixing, and a strong, nutrient-rich boundary current. These processes mediate the nutrient fluxes required to sustain the intense growth of phytoplankton. The resulting biological productivity leads to $CO_2$ drawdown from the atmosphere at rates comparable to some of the largest $CO_2$ sinks in the World Ocean. The fate of this carbon captured from the atmosphere within the PS is largely unknown.

## Key points

Distribution of sea-air $CO_2$ fluxes are analyzed.

Biological and thermal effects on $CO_2$ in the Patagonian Sea are evaluated.

Biological effects dominate the $CO_2$ variability.

## References

Acha, E.M., Mianzan, H.W., Guerrero, R.A., Favero, M., Bava, J., 2004. Marine fronts at the continental shelves of austral South America. Physical and ecological processes. J. Mar. Syst. 44, 83–105. http://dx.doi.org/10.1016/j.jmarsys.2003.09.005.

Atlas, R., Hoffman, R.N., Ardizzone, J., Leidner, S.M., Jusem, J.C., Smith, D.K., Gombos, D., 2011. A cross-calibrated, multiplatform ocean surface wind velocity product for meteorological and oceanographic applications. Bull. Am. Meteor. Soc. 92, 157–174. http://dx.doi.org/10.1175/2010BAMS2946.1.

BaRDO, Base Regional de Datos Oceanográficos. Instituto Nacional de Investigación y Desarrollo Pesquero: Gabinete de Oceanografía Física, -Ministerio de Agricultura Ganadería y Pesca, Subsecretaría de Pesca y Acuicultura de la Nación. Instituto Nacional de Investigación y Desarrollo Pesquero. Paseo Victoria Ocampo N°1, Mar del Plata, Bs. As. Argentina.

Bates, N.R., 2006. Air-sea $CO_2$ fluxes and the continental shelf pump of carbon in the Chukchi Sea adjacent to the Arctic Ocean. J. Geophys. Res. 111, C10013. http://dx.doi.org/10.1029/2005JC003083.

Bates, N.R., Mathis, J.T., Jeffries, M.A., 2011. Air-sea $CO_2$ fluxes on the Bering Sea shelf. Biogeosciences 8, 1237–1253. http://dx.doi.org/10.5194/bg-8-1237-2011.

Bianchi, A.A., Bianucci, L., Piola, A., Ruiz Pino, D., Schloss, I., Poisson, A., Balestrini, C., 2005. Vertical stratification and sea-air $CO_2$ fluxes in the Patagonian shelf. J. Geophys. Res. 110, C07003. http://dx.doi.org/10.1029/2004JC002488.

Bianchi, A.A., Ruiz Pino, D., Isbert Perlender, H.G., Osiroff, A.P., Segura, V., Lutz, V., Clara, M.L., Balestrini, C.F., Piola, A.P., 2009. Annual balance and seasonal variability of sea-air $CO_2$ fluxes in the Patagonia Sea: their relationship with fronts and chlorophyll distribution. J. Geophys. Res. 114, C0301. http://dx.doi.org/10.1029/2008JC004854.

Bogazzi, E., Baldoni, A., Rivas, A., Martos, P., Reta, R., Orensanz, J.L., Lasta, M., Dell'Arciprete, P., Werner, F., 2005. Spatial correspondence between areas of concentration of Patagonian scallop (Zygochlamys patagonica) and frontal systems in the southwestern Atlantic. Fish. Oceanogr. 14 (5), 359–376. http://dx.doi.org/10.1111/j.1365-2419.2005.00340.x.

Borges, A.V., 2011. Present day carbon dioxide fluxes in the coastal ocean and possible feedbacks under global change. In: Oceans and the Atmospheric Carbon Content. Springer Netherlands. doi: http://dx.doi.org/10.1007/978-90-481-9821-4_3, pp. 47-77.

Borges, A.V., Delille, B., Frankignoulle, M., 2005. Budgeting sinks and sources of $CO_2$ in the coastal ocean: diversity of ecosystems counts. Geophys. Res. Lett. 32, L14601. http://dx.doi.org/10.1029/2005GL023053.

Boyer, T.P., Antonov, J. I., Baranova, O. K., Coleman, C., Garcia, H. E., Grodsky, A., Johnson, D. R., Locarnini, R. A., Mishonov, A. V., O'Brien, T. D., Paver, C. R., Reagan, J. R., Seidov, D., Smolyar, I. V., Zweng, M. M., 2013. World ocean database 2013. NOAA Atlas NESDIS 72, Levitus, S. Ed., Mishonov, A. Technical Ed. Silver Spring, MD, 209 pp.

Brandhorst, W., Castello, J.P., 1971. Evaluación de los recursos de anchoíta (Engraulis anchoíta) frente a la Argentina y Uruguay I: las condiciones oceanográficas, sinopsis del conocimiento actual sobre la anchoíta y el plan para su evaluación. Proy. Des. Pesq. Ser. Inf. Tec. 29, 63.

Cai, W.J., 2011. Estuarine and coastal ocean carbon paradox: $CO_2$ sinks or sites of terrestrial carbon incineration? Annu. Rev. Mar. Sci. 3, 123–145. http://dx.doi.org/10.1146/annurev-marine-120709-142723.

Cai, W.J., Wang, Z.A., Wang, Y., 2003. The role of marsh-dominated heterotrophic continental margins in transport of $CO_2$ between the atmosphere, the land-sea interface and the ocean. Geophys. Res. Lett. 301, 1849. http://dx.doi.org/10.1029/2003GL017633.

Cai, W.J., Dai, M.H., Wang, Y.C., 2006. Air–sea exchange of carbon dioxide in ocean margins: a province-based synthesis. Geophys. Res. Lett. 33, L12603. http://dx.doi.org/10.1029/2006GL026219.

Carreto, J.I., Benavides, H.R., Negri, R.M., Glorioso, P.D., 1986. Toxic red-tide in the Argentine Sea. Phytoplankton distribution and survival of the toxic dinoflagellate Gonyaulax excavate in a frontal area. J. Plankton Res. 8, 15–28.

Carreto, J.I., Lutz, V.A., Carignan, M.O., Cucchi Colleoni, A.D., De Marco, S.G., 1995. Hydrography and chlorophyll a in a transect from the coast to the shelf-break in the Argentinian Sea. Cont. Shelf Res. 15 (2), 315–336. http://dx.doi.org/10.1016/0278-4343(94)E0001-3.

Carreto, J.I., Montoya, N.G., Carignan, M.O., Akselman, R., Marcelo Acha, E., Derisio, C., 2016. Environmental and biological factors controlling the spring phytoplankton bloom at the Patagonian shelf-break front - Degraded fucoxanthin pigments and the importance of microzooplankton grazing. Progress Oceanogr.. http://dx.doi.org/10.1016/j.pocean.2016.05.002.

Charo, M., Piola, A.R., 2014. Hydrographic data from the GEF Patagonia Cruises. Earth Syst. Sci. Data 6, 265–271. http://dx.doi.org/10.5194/essd-6-265-2014.

Chen, C.T.A., Andreev, A., Kim, K.R., Yamamoto, M., 2004. Roles of continental shelves and marginal seas in the biogeochemical cycles of the North Pacific Ocean. J. Oceanogr. 60, 17–44. http://dx.doi.org/10.1023/B:JOCE.0000038316.56018.d4.

Chen, C.T.A., Borges, A.V., 2009. Reconciling opposing views on carbon cycling in the coastal ocean: continental shelves as sinks and near-shore ecosystems as sources of atmospheric $CO_2$. Deep-Sea Res. Ii. 56, 578–590. http://dx.doi.org/10.1016/j.dsr2.2009.01.001.ç.

Combes, V., Matano, R.P., 2014. A two-way nested simulation of the oceanic circulation in the Southwestern Atlantic. J. Geophys. Res. Oceans 119, 731–756. http://dx.doi.org/10.1002/2013JC009498.

Copin-Montégut, G., 1996. Chimie de l'Eau de Mer, 319 pp. Inst. Océanogr. de Paris, Paris, France.

DeGrandpre, M.D., Olbu, G.J., Beatty, C.M., Hammar, T.R., 2002. Air–sea $CO_2$ fluxes on the US Middle Atlantic Bight. Deep-Sea Res. II 49, 4355–4367. http://dx.doi.org/10.1016/S0967-0645(02)00122-4.

Dogliotti, A.I., Lutz, V.A., Segura, V., 2014. Estimation of primary production in the southern Argentine continental shelf and shelf-break regions using field and remote sensing data. Remote Sens. Environ. 140, 497–508. http://dx.doi.org/10.1016/j.rse.2013.09.021.

Evans, W., Mathis, J.T., Cross, J.N., Bates, N.R., Frey, K.E., Else, B.G.T., Papkyriakou, T.N., DeGrandpre, M.D., Islam, F., Cai, W.-J., Chen, B., Yamamoto-Kawai, M., Carmack, E., Williams, W.J., Takahashi, T., 2015. Sea-air $CO_2$ exchange in the western Arctic coastal ocean. Glob. Biogeochem. Cycles 29. http://dx.doi.org/10.1002/2015GB005153.

Franco, B.C., Palma, E.D., Combes, V., Lasta, M.L., 2017. Physical processes controlling passive larval transport at the Patagonian Shelf Break Front. J. Sea Res.. http://dx.doi.org/10.1016/j.seares.2017.04.012.

Franco, B.C., Piola, A.R., Rivas, A.L., Baldoni, A., Pisoni, J.P., 2008. Multiple thermal fronts near the Patagonian shelf break. Geophys. Res. Lett. 35, L02607. http://dx.doi.org/10.1029/2007GL032066.

Frankignoulle, M., Borges, A.V., 2001. European continental shelf as a significant sink for atmospheric carbon dioxide. Glob. Biogeochem. Cycles 15, 569–576. http://dx.doi.org/10.1029/2000GB001307.

Garcia, V.M.T., Garcia, C.A.E., Mata, M.M., Pollery, R.C., Piola, A., Signorini, S.R., McClain, C.R., Iglesias-Rodriguez, M.D., 2008. Environmental factors controlling the phytoplankton blooms at the Patagonia shelf-break in spring. Deep-Sea Res. I 55, 1150–1166. http://dx.doi.org/10.1016/j.dsr.2008.04.011.

Glorioso, P.D., 1987. Temperature distribution related to shelf-sea fronts on the Patagonian shelf. Cont. Shelf Res. 7 (1), 27–34. http://dx.doi.org/10.1016/0278-4343(87)90061-6.

Gómez, M.I., Piola, A., Kattner, G., Alder, V.A., 2011. Biomass of autotrophic dinoflagellates under weak vertical stratification and contrasting chlorophyll levels in subantarctic shelf waters. J. Plankton Res. 33 (8), 1304–1310.

Guo, X.-H., Zhai, W.-D., Dai, M.-H., Zhang, C., Bai, Y., Xu, Y., Li, Q., Wang, G.-Z., 2015. Air–sea $CO_2$ fluxes in the East China Sea based on multiple-year underway observations. Biogeosciences 12, 5495–5514. http://dx.doi.org/10.5194/bg-12-5495-2015.

Holm-Hansen, O., Lorenzen, C.J., Holmes, R.W., Strickland, J.D.H., 1965. Fluorometric determination of chlorophyll. J. Cons. 30 (1), 3–15. http://dx.doi.org/10.1093/icesjms/30.1.3.

Ito, R.G., Schneider, B., Thomas, H., 2005. Distribution of surface $fCO_2$ and air–sea fluxes in the South western subtropical Atlantic and adjacent continental shelf. J. Mar. Syst. 56, 227–242. http://dx.doi.org/10.1016/j.jmarsys.2005.02.005.

Jiang, L.-Q., Cai, W.-J., Wanninkhof, R., Wang, Y., Lüger, H., 2008. Air–sea $CO_2$ fluxes on the U.S. South Atlantic Bight: spatial and seasonal variability. J. Geophys. Res. 113, C07019. http://dx.doi.org/10.1029/2007JC004366.

Kahl, L.C., 2013. Balance y variabilidad del $CO_2$ en el Mar Patagónico (Thesis). Universidad de Buenos Aires, Argentina, 115.

Kim, D., Choi, S.H., Shim, J., Kim, K.H., Kim, C.H., 2013. Revisiting the seasonal variations of sea-air $CO_2$ fluxes in the northern East China Sea. Terr. Atmos. Ocean. Sci. 24, 409–419. http://dx.doi.org/10.3319/TAO.2012.12.06.01(Oc).

Laruelle, G.G., Lauerwald, R., Pfeil, B., Regnier, P., 2014. Regionalized global budget of the $CO_2$ exchange at the air-water interface in continental shelf seas. Glob. Biogeochem. Cycles 28, 1199–1214. http://dx.doi.org/10.1002/2014GB004832.

Le Quéré, C., Andrew, R.M., Canadell, J.G., Sitch, S., Korsbakken, J.I., Peters, G.P.,

Manning, A.C., Boden, T.A., Tans, P.P., Houghton, R.A., Keeling, R.F., Alin, S., Andrews, O.D., Anthoni, P., Barbero, L., Bopp, L., Chevallier, F., Chini, L.P., Ciais, P., Currie, K., Delire, C., Doney, S.C., Friedlingstein, P., Gkritzalis, T., Harris, I., Hauck, J., Haverd, V., Hoppema, M., Klein Goldewijk, K., Jain, A.K., Kato, E., Körtzinger, A., Landschützer, P., Lefèvre, N., Lenton, A., Lienert, S., Lombardozzi, D., Melton, J.R., Metzl, N., Millero, F., Monteiro, P.M.S., Munro, D.R., Nabel, J.E.M.S., Nakaoka, S.-I., O'Brien, K., Olsen, A., Omar, A.M., Ono, T., Pierrot, D., Poulter, B., Rödenbeck, C., Salisbury, J., Schuster, U., Schwinger, J., Séférian, R., Skjelvan, I., Stocker, B.D., Sutton, A.J., Takahashi, T., Tian, H., Tilbrook, B., van der Laan-Luijkx, I.T., van der Werf, G.R., Viovy, N., Walker, A.P., Wiltshire, A.J., Zaehle, S., 2016. Global Carbon Budget 2016. Earth Syst. Sci. Data 8, 605–649. http://dx.doi.org/10.5194/essd-8-605-2016.

Lucas, A.J., Guerrero, R.A., Mianzan, M.W., Acha, E.M., Lasta, C.A., 2005. Coastal oceanographic regimes of the Northern Argentine Continental Shelf (34–43°S). Estuar. Coast. Shelf Sci. 65, 405–420. http://dx.doi.org/10.1016/j.ecss.2005.06.015.

Lutz, V.A., Segura, V., Dogliotti, A.I., Gagliardini, D.A., Bianchi, A.A., Balestrini, C.F., 2010. Primary production in the Argentine Sea during spring estimated by field and satellite models. J. Plankton Res. 32, 181–195. http://dx.doi.org/10.1093/plankt/fbp117.

Marrari, M., Signorini, S.R., Mc Clain, C.R., Pájaro, M., Martos, P., Viñas, M.D., Hansen, J., Dimauro, R., Cepeda, G., Buratti, C., 2013. Reproductive success of the Argentine anchovy, Engraulis anchita, in relation to environmental variability at a mid-shelf front (Southwestern Atlantic Ocean). Fish. Oceanogr. 22, 247–261. http://dx.doi.org/10.1111/fog.12019.

Matano, R.P., Combes, V., Piola, A.R., Guerrero, R., Palma, E.D., Ted Strub, P., James, C., Fenco, H., Chao, Y., Saraceno, M., 2014. The salinity signature of the cross-shelf exchangesin the Southwestern Atlantic Ocean: numerical simulations. J. Geophys. Res. Oceans 119, 7949–7968. http://dx.doi.org/10.1002/2014JC010116.

Matano, R.P., Palma, E.D., 2008. On the upwelling of downwelling currents. J. Phys. Oceanogr. 38 (11), 2482–2500. http://dx.doi.org/10.1175/2008JPO3783.1.

Mathis, J.T., Cross, J.N., Bates, N.R., Bradley Moran, S., Lomas, M.W., Mordy, C.W., Stabeno, P.J., 2010. Seasonal distribution of dissolved inorganic carbon and net community production on the Bering Sea shelf. Biogeosciences 7, 1769–1787. http://dx.doi.org/10.5194/bg-7-1769-2010.

Metzl, N., Poisson, A., Louanchi, F., Brunet, C., Schauer, B., Bres, B., 1995. Spatio-temporal distributions of sea-air fluxes of $CO_2$ in the Indian and Antarctic oceans: a first step. Tellus B 47, 56–60.

Miller, R.N., Matano, R.P., Palma, E.D., 2011. Shelf break upwelling induced by alongshore currents: analytical and numerical results. J. Fluid Mech. 686, 239–249.

Palma, E.D., Matano, R.P., Piola, A.R., 2008. A numerical study of the Southwestern Atlantic Shelf circulation: stratified ocean response to local and offshore forcing. J. Geophys. Res. 113, C11010. http://dx.doi.org/10.1029/2007JC004720.

Pierrot, D., Lewis, E., Wallace, D.W.R., 2006. MS Excel Program Developed for $CO_2$ System Calculations. ORNL/CDIAC-105a. Carbon Dioxide Information Analysis Center, Oak Ridge National Laboratory, U.S. Department of Energy, Oak Ridge, Tennessee. http://dx.doi.org/10.3334/CDIAC/otg.CO2SYS_XLS_CDIAC105a.

Piola, A.R., Rivas, A.L., 1997. Corrientes en la plataforma continental, In: El Mar Argentino y sus Recursos Pesqueros, Antecedentes Históricos de las Exploraciones en el Mar y las Características Ambientales. Editorial: E. E. Boschi., 1, pp. 119–132.

Piola, A.R., Möller, O.O., Guerrero, R.A., Campos, E.J., 2008. Variability of the subtropical shelf front off eastern South America: winter 2003 and summer 2004. Cont. Shelf Res. 28, 1639–1648. http://dx.doi.org/10.1016/j.csr.2008.03.013.

Piola, A.R., Franco, B.C., Palma, E.D., Saraceno, M., 2013. Multiple jets in the Malvinas Current. J. Geophys. Res. 118 (4), 2107–2117. http://dx.doi.org/10.1002/jgrc.20170.

Podestá, G.P., Brown, O.B., Evans, R.H., 1991. The annual cycle of satellite-derived sea surface temperature in the Southwestern Atlantic Ocean. J. Clim. 4, 457–467.

Prowe, A.E.F., Thomas, H., Pätsch, J., Kühn, W., Bozec, Y., Schiettecatte, L.S., Borges, A.V., de Baar, H.J.W., 2009. Mechanisms controlling the air–sea $CO_2$ flux in the North Sea. Cont. Shelf Res. 29 (15), 1801–1808. http://dx.doi.org/10.1016/j.csr.2009.06.003.

Rivas, A.L., 1997. Current-meter observations in the Argentine Continental Shelf. Cont. Shelf Res. 17 (4), 391–406. http://dx.doi.org/10.1016/S0278-4343(96)00039-8.

Rivas, A.L., 2010. Spatial and temporal variability of satellite-derived sea surface temperature in the southwestern Atlantic Ocean. Cont. Shelf Res. 30 (7), 752–760. http://dx.doi.org/10.1016/j.csr.2010.01.009.

Rivas, A.L., Piola, A.R., 2002. Vertical stratification at the shelf off northern Patagonia. Cont. Shelf Res. 22 (10), 1549–1558. http://dx.doi.org/10.1016/S0278-4343(02)00011-0.

Rivas, A.L., Dogliotti, A.I., Gagliardini, D.A., 2006. Seasonal variability in satellite-measured surface chlorophyll in the Patagonian Shelf. Cont. Shelf Res. 26 (6), 703–720. http://dx.doi.org/10.1016/j.csr.2006.01.013.

Rivas, A.L., Pisoni, J.P., 2010. Identification, characteristics and seasonal evolution of surface thermal fronts in the Argentinean Continental Shelf. J. Mar. Syst. 79, 134–143. http://dx.doi.org/10.1016/j.jmarsys.2009.01.008.

Romero, S.I., Piola, A.R., Charo, M., Eiras García, C.A., 2006. Chlorophyll a variability off Patagonia based on SeaWiFS data. J. Geophys. Res. 111, C05021. http://dx.doi.org/10.1029/2005JC003244.

Rubin, S.I., 2000. Processes Controlling the Distribution of Carbon Dioxide and Nutrients in the South Pacific and Southern Oceans (Ph.D. Thesis). Columbia University, New York, NY, 223.

Ruiz Etcheverry, L.A., Saraceno, M., Piola, A.R., Strub, P.T., 2016. Sea level anomaly on the Patagonian continental shelf: trends, annual patterns and geostrophic flows. J. Geophys. Res.. http://dx.doi.org/10.1002/2015JC011265.

Sabatini, M.E., Ramírez, F.C., Martos, M., 2000. Distribution pattern and population structure of Calanus australis Brodsky, 1959 over the southern Patagonian shelf off

Argentina in summer. ICES J. Mar. Sci. 57, 1856–1866. http://dx.doi.org/10.1006/jmsc.2000.0969.

Sabatini, M., Reta, R., Matano, R., 2004. Circulation and zooplankton biomass distribution over the southern Patagonian shelf during late summer. Cont. Shelf Res. 24 (12), 1359–1373. http://dx.doi.org/10.1016/j.csr.2004.03.014.

Sabatini, M.E., Akselman, R., Reta, R., Negri, R.M., Lutz, V.A., Silva, R.I., Segura, V., Gil, M.N., Santinelli, N.H., Sastre, A.V., Daponte, M.C., Antacli, J.C., 2012. Spring plankton communities in the southern Patagonian shelf: hydrography, mesozooplankton patterns and trophic relationships. J. Mar. Syst. 94, 33–51. http://dx.doi.org/10.1016/j.jmarsys.2011.10.007.

Schejter, L., Bremec, C., Akselman, R., Hernandez, D., Spivak, E., 2002. Annual feeding cycle of the Patagonian scallop Zigochlamyspatagonica (King and Broderip, 1832) in Recludas bed (39S-55W). Argent. Sea J. Shellfish Res. 21, 553–559.

Schloss, I.R., Ferreyra, G.A., Ferrario, M.E., Almandoz, G.O., Codina, R., Bianchi, A.A., Balestrini, C.F., Ochoa, H.A., Ruiz Pino, D., Poisson, A., 2007. Role of plankton communities in sea-air differences in $p$CO$_2$ in the SW Atlantic Ocean. Mar. Ecol. Prog. Ser. 332, 93–106. http://dx.doi.org/10.3354/meps332093.

Signorini, S.R., Garcia, V.M.T., Piola, A.R., Evangelista, H., McClain C.R., Garcia, C.A.E., Mata, M.M., 2009. Further studies on the physical and biogeochemical causes for large interannual changes in the Patagonian shelf spring–summer phytoplankton bloom biomass. NASA Technical Memorandum, NASA/TM-2009-214176, Greenbelt, MD, 43 pp.

Simpson, J.H., 1981. The shelf-sea fronts: implications of their existence and behavior. Philos. Trans. R. Soc. Lond. Ser. A 302, 531–546.

Song, H., Marshall, J., Follows, M.J., Dutkiewicz, S., Forget, G., 2016. Source waters for the highly productive Patagonian shelf in the southwestern Atlantic. J. Mar. Syst. 158, 120–128. http://dx.doi.org/10.1016/j.jmarsys.2016.02.009.

Strickland, J.D.H., Parsons, T. R., 1972. A practical handbook of seaweater analysis, Bull. 167, 311 pp., Fish. Res. Board of Can., Ottawa, Ont., Canada.

Strub, P.T., James, C., Combes, V., Matano, R.P., Piola, A.R., Palma, E.D., Saraceno, M., Guerrero, R.A., Fenco, H., Ruiz-Etcheverry, L.A., 2015. Altimeter-derived seasonal

circulation on the southwest Atlantic shelf: 278– 438S. J. Geophys. Res. Oceans 120, 3391–3418. http://dx.doi.org/10.1002/2015JC010769.

Takahashi, T., Olafsson, J., Goddard, J., Chipman, D.W., Sutherland, S.C., 1993. Seasonal variation of CO$_2$ and nutrients in the high-latitude surface oceans: a comparative study. Glob. Biogeochem. Cycles 7, 843–878.

Takahashi, T., Sutherland, S.C., Sweeney, C., Poisson, A., Metzl, N., Tilbrook, B., Bates, N., Wanninkhof, R., Feely, R.A., Sabine, C., Olafsson, J., Nojiri, Y., 2002. Global sea-air CO$_2$ fluxes based on climatological surface ocean $p$CO$_2$, and seasonal biological and temperature effects. Deep-Sea Res. II 49, 1601–1622. http://dx.doi.org/10.1016/S0967-0645(02)00003-6.

Thomas, H., Bozec, Y., Elkalay, K., De Baar, H.J., 2004. Enhanced open ocean storage of CO$_2$ from shelf sea pumping. Science 304, 1005–1008. http://dx.doi.org/10.1126/science.1095491.

Tsunogai, S., Watanabe, S., Sato, T., 1999. Is there a "continental shelf pump" for the absorption of atmospheric CO$_2$? Tellus B 5, 701–712. http://dx.doi.org/10.1034/j.1600-0889.1999.t01-2-00010.x.

Valla, D., Piola, A.R., 2015. Evidence of upwelling events at the northern Patagonian shelf break. J. Geophys. Res. Oceans 120. http://dx.doi.org/10.1002/2015JC011002.

Volk, T., Hoffert, M.I., 1985. Ocean carbon pumps: Analysis of relative strengths and efficiencies in ocean-driven atmospheric CO$_2$ changes. In: The Carbon Cycle and Atmospheric CO$_2$: Natural Variations Archean to Present. Geophysical Monograph Vol. 32, American Geophysical Union, Washington DC, pp. 99–110.

Walsh, J.J., 1988. On the Nature of Continental Shelves. Academic, San Diego, 520.

Wang, S.L., Chen, C.T.A., Hong, G.H., Chung, C.S., 2000. Carbon dioxide and related parameters in the East China Sea. Cont. Shelf Res. 20, 525–544. http://dx.doi.org/10.1016/S0278-4343(99)00084-9.

Wanninkhof, R., 2014. Relationship between wind speed and gas exchange over the ocean revisited. Limnol. Oceanogr.: Methods 12 (6), 351–362. http://dx.doi.org/10.4319/lom.2014.12.351.